Climate change dominates the increasing exposure of global population to compound heatwave and humidity extremes in the future

Yiheng Wei
weiyiheng@whu.edu.cn
Wuhan University https://orcid.org/0009-0009-9245-1960
Dunxian She
Wuhan University
Jun Xia
Wuhan University
Gangsheng Wang
Wuhan University
Qin Zhang
Changjiang River Scientific Research Institute
Shengzhi Huang
Xi'an University of Technology
Yu Zhang
Beijing Normal University
Tianyue Wang
Wuhan University

Research Article

Keywords: climate change, compound heatwave and humidity extremes, CMIP6

Posted Date: February 6th, 2024

DOI: https://doi.org/10.21203/rs.3.rs-3378606/v1

Version of Record: A version of this preprint was published at Climate Dynamics on April 5th, 2024. See the published version at https://doi.org/10.1007/s00382-024-07199-x.

Climate change dominates the increasing exposure of global population to compound heatwave and humidity extremes in the future

Yiheng Wei[1,2], Dunxian She[1,2,*], Jun Xia[1,2], Gangsheng Wang[1,2], Qin Zhang[1,3], Shengzhi Huang[4], Yu Zhang[5], Tianyue Wang[1,2]

1. State Key Laboratory of Water Resources Engineering and Management, Wuhan University, Wuhan, Hubei, 430072, P.R. China

2. Hubei Key Laboratory of Water System Science for Sponge City Construction, Wuhan University, Wuhan, 430072, P.R. China

3. Changjiang River Scientific Research Institute of Changjiang Water Resources Commission, Wuhan, 430010, P.R. China

4. State Key Laboratory of Eco-Hydraulics in Northwest Arid Region of China, Xi'an University of Technology, Xi'an, 710048, P.R. China

5. College of Water Sciences, Beijing Normal University, Beijing, 100875, P.R. China

Corresponding author: Dr. Dunxian She (shedunxian@whu.edu.cn)

Abstract

Under global warming, compound event arises increasing attract as it can lead to a growing impact on water resources management, human society, and ecosystem, especially for the compound heatwave and humidity extremes (CHHE), which can exert harmful influence on human health. However, the understanding of changes in CHHE both in the historical and future, and attribution of global population exposure to CHHE are far from enough. In this study, we selected the wet-bulb temperature (T_w) to define the CHHE, and used the Coupled Model Intercomparison Project Phase 6 (CMIP6) data to investigate future changes in global CHHE. Furthermore, we quantified the relative contributions of population, climate change and their interaction effect to the change in population exposure to CHHE. We found that all scenarios (SSP1-2.6, SSP2-4.5, SSP3-7.0 and SSP5-8.5) show an increasing trend of CHHE. For SSP5-8.5, the global mean T_w will increase by 7°C, and the northern North America and central Africa experience warming approaching 10°C by the end of 21st century. Under SSP3-7.0 and SSP5-8.5, large equatorial regions will witness T_w exceeding 35°C resulting in an exposure of 10^5 million person-days. All the scenarios presented an increase in population exposure to CHHE, which is mainly contributed by climate change (50%-90%) rather than population under different scenarios. We also found that the contribution of population-climate interaction is significantly higher in Africa than in other regions, which mainly due to high population growth rates in the future. Our study provides scientific basis

and useful information for the development of adaptation strategies to reduce disaster risks caused by CHHE.

Highlights

(1) Wet bulb temperature is projected to increase significantly under different scenarios.

(2) Population exposure in equatorial area will rise under high emission scenarios.

(3) Climate change dominants the increase in global population exposure.

Keywords

climate change; compound heatwave and humidity extremes; CMIP6

1 Introduction

Under climate change, the frequency and/or intensity of various extremes (such as heatwaves, droughts, and heavy precipitations) increases, causing huge loss of life and economic damage (*IPCC*, 2021; *Kurz et al.*, 2008; *Lesk et al.*, 2017). For instance, 2003 European heatwave event killed tens of thousands of people and the 2010 Russian heatwave event led to higher global food prices than normal years (*Haines et al.*, 2006; *Wegren*, 2013). In the future, global warming will continue due to human emissions of greenhouse gases, and the frequency and intensity of heatwave will continue to increase, projected to affect more people (*Byrne and O'Gorman*, 2018). Research on extreme events has received significant attention in recent years due to their severe impact on human societies and economies (*Alexander et al.*, 2006; *Cook et al.*, 2020; *Q Zhang et al.*, 2022). Compound events can be defined as two or more extreme events occurring simultaneously or successively, such as compound flood and hot events (Gu et al., 2022), combination of tropical cyclones and moist heat (Rajeev & Mishra, 2022), compound drought and heatwave events (Zhang et al., 2022) and compound heatwave and humidity (IPCC, 2021; Coffel et al., 2018). Compared with single extreme events, compound extremes may have more devastating effects on water resources management, human society and ecosystem (*Ridder et al.*, 2020; *Rogers et al.*, 2021; *Zscheischler et al.*, 2018; *Tripathy et al.*, 2023). Specially, the compound heat and humidity extremes (CHHE), which can be defined as the co-occurrence of heatwave and high humidity, have much more severe threat to human than single heatwave event

(*Coffel et al.*, 2018; *Raymond et al.*, 2020). Some studies suggested that heat-humidity extremes have increased faster and effect more people than heat extremes (*Li*, 2020; *Rogers et al.*, 2021). Recent researches found that both high temperature and humidity caused the high mortality in India and Pakistan during the 2015 heatwave event (*Wehner, Stone, Krishnan, AchutaRao, & Castillo*, 2016). With the acceleration of urbanization, anthropogenic heat emission will increase, which can aggravate urban heat island (*Huang, Song, Wang, Chui, & Chan*, 2021). The use of cooling and dehumidifying facilities leads to increase urban moisture island (*Shi et al.*, 2019). The hot and humidity cities will regulate region climate and increase heat-related morbidity and mortality. Hence, it is essential to investigate the exposure of global population to compound heatwave and humidity extremes, which is beneficial to provide useful information for the development of adaptation strategies.

CHHE affect human body through multiple factors, such as temperature, humidity, wind speed, radiation, human's activities and clothing. The heat index (such as wet-bulb temperature (T_w), wet bulb globe temperature (WBGT), discomfort index (DI), and etc.) is widely used to quantify CHHE (*Epstein & Moran*, 2006; *Li*, 2020; *Sherwood & Huber*, 2010). Most of heat indices focused on how to measure the high air temperature and high humidity conditions as both temperature and humidity affect the heat exchange between the human body and the environment (*Petkova et al.*, 2013). At high air temperature, the human body can effectively dissipate heat through evaporation if the humidity is low, but the human body becomes less efficient at evaporating heat with high temperature and high humidity conditions, which can increase body temperature and eventually lead to heat stroke or even death (*Raymond et al.*, 2020). The threat to human health from heatwave events cannot be accurately assessed if only air temperature is considered (*Diffenbaugh et al.*, 2007; *Dunne et al.*, 2013; *Fischer and Schär*, 2010). Some heat indexes (such as WBGT) consider many variables such as wind speed, radiation, air temperature, humidity, and these indices may characterize heat stress to human body theoretically. However, the data needed in these index are often limited in availability and quality (*Rogers* et al., 2021). Previous studies also suggested that the ambient heat stress reflected by WBGT is strongly influenced by clothing and human activity, while T_w establishes clear thermodynamic limits that eliminate these effects (*Sherwood and Huber*, 2010). Numerous studies have been conducted to analyze the heatwave event at different scales using T_w. Under current climate conditions, T_w rarely exceeds 35°C (*Pal and Eltahir*, 2016; *Raymond et al.*, 2020; *Schär*, 2016). Some studies suggest that T_w will exceed 35°C in South Asia and the Middle East (*Im et al.*, 2017; *Pal and Eltahir*, 2015), and the number of high-risk days will increase 10-30% in West, Central and Northeast Africa by the end of the 21st century (*Fotso-Nguemo et al.*, 2023).

Population exposure is a common metric to assess the impact of compound events on human society (*Feng et al.*, 2022; *Yu and Zhai*, 2020). For example, Li et al. (2020) speculate that1.22 billion people will be exposed to extreme wet heat events if the globe warms by 3°C. Population exposure is affected by both climate change and population change (*G. Zhang et al.*, 2022). Coffel et al. (2018) suggested that changes in global extreme humidity and heatwave events mainly caused by population change, climate change, and the population-climate interactions, and they concluded that the increase in global exposure was largely attributable to climate change. Similar work given by Chen et al. (2022) also concluded that the contribution of population change was almost zero in China. We can find that the conclusions from the previous studies on the contribution proportion of population-climate interactions are inconsistent under different regions and scenarios.

Generally, previous studies mainly focused on the regional change of CHHE during the historical or future period. Although almost all the studies suggested CHHE is experiencing rapidly increasing trend during the historical period and will continue to increase in the future, there are serval studies evaluating the projection characteristics globally, and only limit future scenarios (representative concentration pathways, RCP 4.5 and RCP 8.5) were selected (*Ballester et al.*, 2023; *Rogers et al.*, 2021; *Wehner, Stone, Krishnan, AchutaRao, & Castillo*, 2016). Such as Coffel et al. (2018) evaluated the change of CHHE and population exposure using CMIP5 data under RCP 4.5 and RCP 8.5. With the development of CMIP6 data, the higher resolution and improved physical processes data can be used to projected future change (*Zhang et al.*, 2022). Chen et al. (2022) used CMIP6 data to evaluate the change of CHHE under four Shared Socioeconomic Pathway (SSP) scenarios in China. However, the understanding of change of population exposure is far from enough, especially lacks the further assessment of the spatially variability in different regions and their contributing factors of population exposure to CHHE changes.

In this study, we calculated the global T_w and population exposure of CHHE in historical (1979-2014) and various future (2015-2100) scenarios (i.e., SSP-RCP scenario) using CMIP6 data. Furthermore, we quantitatively attributed the changes in exposure into three components, i.e., population change, climate change, and population-climate interactions in different regions and future time periods. The objectives of the study include: (a) reveal the spatial and temporal patterns of global historical and future CHHE, (b) investigate the effects of CHHE on human society, (c) attribution analysis of population exposure to CHHE. Our study can provide a theoretical basis for improving population adaptive capacity and developing mitigation measures.

2 Materials and Methods

2.1 Data

We used a multi-model ensemble containing 10 GCMs from CMIP6 in this study (Table 1). To calculate the daily T_w, we downloaded daily maximum air temperature (T_{max}), surface pressure (p) and relative humidity (H_r) for the historical simulation period (1979-2014) and future period (2015-2100) under four scenarios (SSP1-2.6, SSP2-4.5, SSP3-7.0, SSP5-8.5) from the GCMs (*Bardon et al.*, 2021; *O'Neill et al.*, 2016; *Riahi et al.*, 2017). Global population data is obtained from the

International Institute for Applied Systems Analysis (IIASA), including 182 countries and territories worldwide under four SSP scenarios which resolution is 0.5°×0.5° (*Kc and Lutz*, 2017).

The global land daily gridded maximum temperature product provided by Climate Prediction Center (CPC-Unified) for the period from 1979 to 2014 with a spatial resolution of 0.5°×0.5° is used to validate the GCM's outputs. The CPC-Unified dataset is widely used in hydrometeorological studies due to its strict quality control and high accuracy (*Mukherjee and Mishra*, 2021; *Nashwan et al.*, 2019; *Tarek et al.*, 2021). The daily surface pressure relative humidity data from ERA5 (the fifth generation of European Center for Medium Weather Forecasting atmospheric reanalysis) is also used to calculate daily T_w. Both CMIP6 model data and observed data were re-gridded to 0.5°×0.5° using bilinear interpolation.

We used the Quantile Mapping (QM) method (*Cannon et al.*, 2015; *Maraun*, 2013) to correct the daily maximum temperature and relative humidity data of CMIP6 based on CPC-unified and ERA5 data. The QM method has been widely used in the bias correction of climate data due to its accuracy and simplicity (*Maurer et al.*, 2010; *Tang et al.*, 2021; *Thrasher et al.*, 2012). And we use root mean square error (RMSE) to assess the performance of bias correction (a smaller value of RMSE suggests a better performance of the bias correction). Additionally, we used 44 global land regions from IPCC AR6 (*IPCC*, 2021) to assess the spatial variability of CHHE (Figure 1).

Table 1 Selected CMIP6 models in this study

Model	Organization	Resolution
CanESM5	Canadian Centre for Climate Modelling and Analysis, Canada	128×64
EC-Earth3	EC-Earth-Consortium	512×256
IPSL-CM6ALR	Institute Pierre-Simon Laplace, France	144×143
KACE-1-0-G	National Institute of Meteorological Sciences/ Korea Meteorological Administration, Climate Research Division, Republic of Korea	192×144
MIROC6	Japan Agency for Marine-Earth Science and Technology, Japan/ Atmosphere and Ocean Research Institute, The University of Tokyo, Japan/ National Institute for Environmental Studies/ RIKEN Center for Computational Science, Japan	256×128
MPI-ESM1-2-HR	Max Planck Institute for Meteorology, Germany	192×96
MPI-ESM1-2-LR	Max Planck Institute for Meteorology, Germany	320×160
NorESM2-LM	Norwegian Climate Centre, Norway	144×96
NorESM2-MM	Norwegian Climate Centre, Norway	288×192
UKESM1-0-LL	National Centre for Atmospheric Science, UK/ Met Office Hadley Centre, UK	192×144

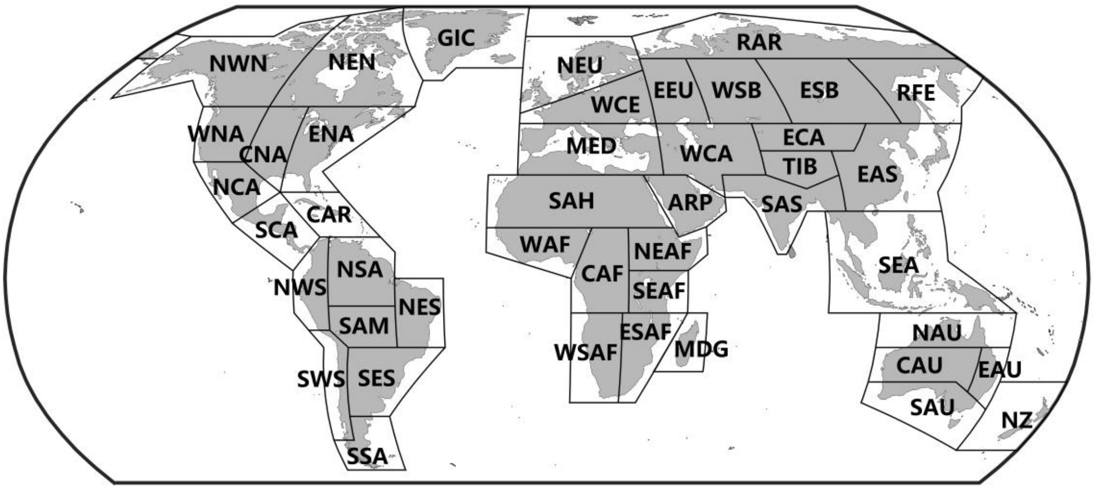

GIC: Greenland/Iceland
NWN: N.W.North-America
NEN: N.E.North-America
WNA: W.North-America
CNA: C.North-America
ENA: E.North-America
NCA: N.Central-America
SCA: S.Central-America
CAR: Caribbean
NWS: N.W.South-America
NSA: N.South-America
NES: N.E.South-America
SAM: South-American-Monsoon
SWS: S.W.South-America
SES: S.E.South-America
SSA: S.South-America
NEU: N.Europe
WCE: Western&Central-Europe
EEU: E.Europe
MED: Mediterranean
SAH: Sahara
WAF: Western-Africa
CAF: Central-Africa
NEAF: N.Eastern-Africa
SEAF: S.Eastern-Africa
WSAF: W.Southern-Africa
ESAF: E.Southern-Africa
MDG: Madagascar
RAR: Russian-Arctic
WSB: W.Siberia
ESB: E.Siberia
RFE: Russian-Far-East
WCA: W.C.Asia
ECA: E.C.Asia
TIB: Tibetan-Plateau
EAS: E.Asia
ARP: Arabian-Peninsula
SAS: S.Asia
SEA: S.E.Asia
NAU: N.Australia
CAU: C.Australia
EAU: E.Australia
SAU: S.Australia
NZ: New-Zealand

Figure 1 Geographic location and description of 44 land regions derived from IPCC AR6 (*IPCC*, 2021)

2.2 Definition of Compound Heatwave and Humidity Extremes

We used T_w to measure the intensity of compound heatwave and humidity extremes. T_w was calculated by the algorithm proposed by Davies-Jones (*Davies-Jones*, 2008). When the daily ambient T_w is greater than 35°C, the evaporative heat dissipation efficiency of the human body through the skin will be greatly reduced and the body will not be able to maintain a stable body temperature (*H. Chen et al.*, 2022). To maintain the body temperature at 37°C, T_w needs to be less than 35°C (*Pal and Eltahir*, 2015; *Sherwood and Huber*, 2010). However, data from the 2003 European heatwave showed that a T_w of around 30°C can cause thousands of human deaths (*Fouillet et al.*, 2008), and empirical data show that working outdoors above 32°C is also very dangerous (*Buzan et al.*, 2015; *Liang et al.*, 2011). Therefore, we mainly investigated the change in T_w with threshold exceeding T_w 35°C and we also explore the case of T_w exceed 32°C as supplementary analysis in this study. This provides an early warning for vulnerable people, such as children and the elderly, in these areas, as well as an indication of higher-risk areas in the future.

The calculation of T_w is given as follows:

$$T_w = \begin{cases} T_E - 273.15 - \dfrac{2675 * r_s}{1 + 2675 * r_s * d\ln(T_E)/dT_E} & \left(\dfrac{273.15}{T_E}\right)^{3.504} > D(\pi) \\ k_1(\pi) - k_2(\pi)(273.15/T_E)^{3.504} & 1 \le \left(\dfrac{273.15}{T_E}\right)^{3.504} \le D(\pi) \\ (k_1(\pi) - 1.21) - (k_2(\pi) - 1.21)\left(\dfrac{273.15}{T_E}\right)^{3.504} & 0.4 \le \left(\dfrac{273.15}{T_E}\right)^{3.504} < 1 \\ (k_1(\pi) - 2.66) - (k_2(\pi) - 1.21)\left(\dfrac{273.15}{T_E}\right)^{3.504} + 0.58\left(\dfrac{273.15}{T_E}\right)^{-3.504} & \left(\dfrac{273.15}{T_E}\right)^{3.504} < 0.4 \end{cases} \quad (1)$$

$$r_s = 610.78 e^{\frac{17.27(T_{\max} - 273.15)}{T_{\max} - 35.86}} \quad (2)$$

$$T_E = T + 1.95 * \frac{r_s * H_R}{100T} \quad (3)$$

$$k_1(\pi) = -38.5\pi^2 + 137.81\pi - 53.737 \quad (4)$$

$$k_2(\pi) = -4.392\pi^2 + 56.831\pi - 0.384 \quad (5)$$

$$D(p) = (0.1859 p / p_0 + 0.6512)^{-1} \quad (6)$$

$$\pi = (p / p_0)^{-3.504} \quad (7)$$

where T_w is wet bulb temperature (K), T_E is equivalent temperature (K), r_s is saturation mixing ratio calculated by T_{max}, H_R is relative humidity, p is surface pressure (Pa), p_0 is standard atmospheric pressure (Pa).

2.3 Attribution of Population Exposure to CHHE

Population exposure is defined as the product of the number of compound event days and the number of people in each pixel (*H. Chen and Sun*, 2021; *Tuholske et al.*, 2021). We used the approach developed by Jones et al. (2015) to analyze the contribution of population and climate change to the increase of population exposure, which has been widely applied to the attribution analysis of extreme events (*Ullah et al.*, 2022; *Weber et al.*, 2020). We attribute the change of population exposure to three parts: population change, climate change and population-climate interactions:

$$\Delta E = CE_H \times \Delta P + P_H \times \Delta CE + \Delta P \times \Delta CE + \delta \quad (8)$$

where ΔE represents the change of population exposure, CE_H and P_H represent the occurrence of compound events and population in the historical period, and ΔCE and ΔP represent their change in the future compared to the historical period, δ represent data bias. The contribution rate of each item can be calculated as follows:

$$CR_P = \frac{CE_H \times \Delta P}{\Delta E} \times 100\% \quad (9)$$

$$CR_{clim} = \frac{P_H \times \Delta CE}{\Delta E} \times 100\% \quad (10)$$

$$CR_{int} = \frac{\Delta P \times \Delta CE}{\Delta E} \times 100\% \quad (11)$$

where CR_P, CP_{clim} and CR_{int} represent the contribution rate of population change, climate change and population-climate interactions, respectively.

3 Results and discussions

3.1 Projected Changes in T_w characteristics

We first examine the performance of the raw and corrected multi-model ensembles average in simulating the T_{max} and H_r (Figure 1). For T_{max}, we find the raw CMIP6 data tends to underestimate the annual average. According to Figure 1b, QM method is better for high temperature corrections. As this study mainly focuses on mid to low latitude regions, the effect of the poorer correction in low temperature on the results can be ignored. For H_r, we find that the raw CMIP6 data slightly overestimates the annual average, and the correction effectively reduces the error. Overall, the QM method effectively reduces the RMSE of the model data and the corrected CMIP6 data can simulate the T_{max} and H_r of the historical period well, so we speculate that it is reasonable to use the corrected CMIP6 data to calculate the future compound extremes (Figure 2).

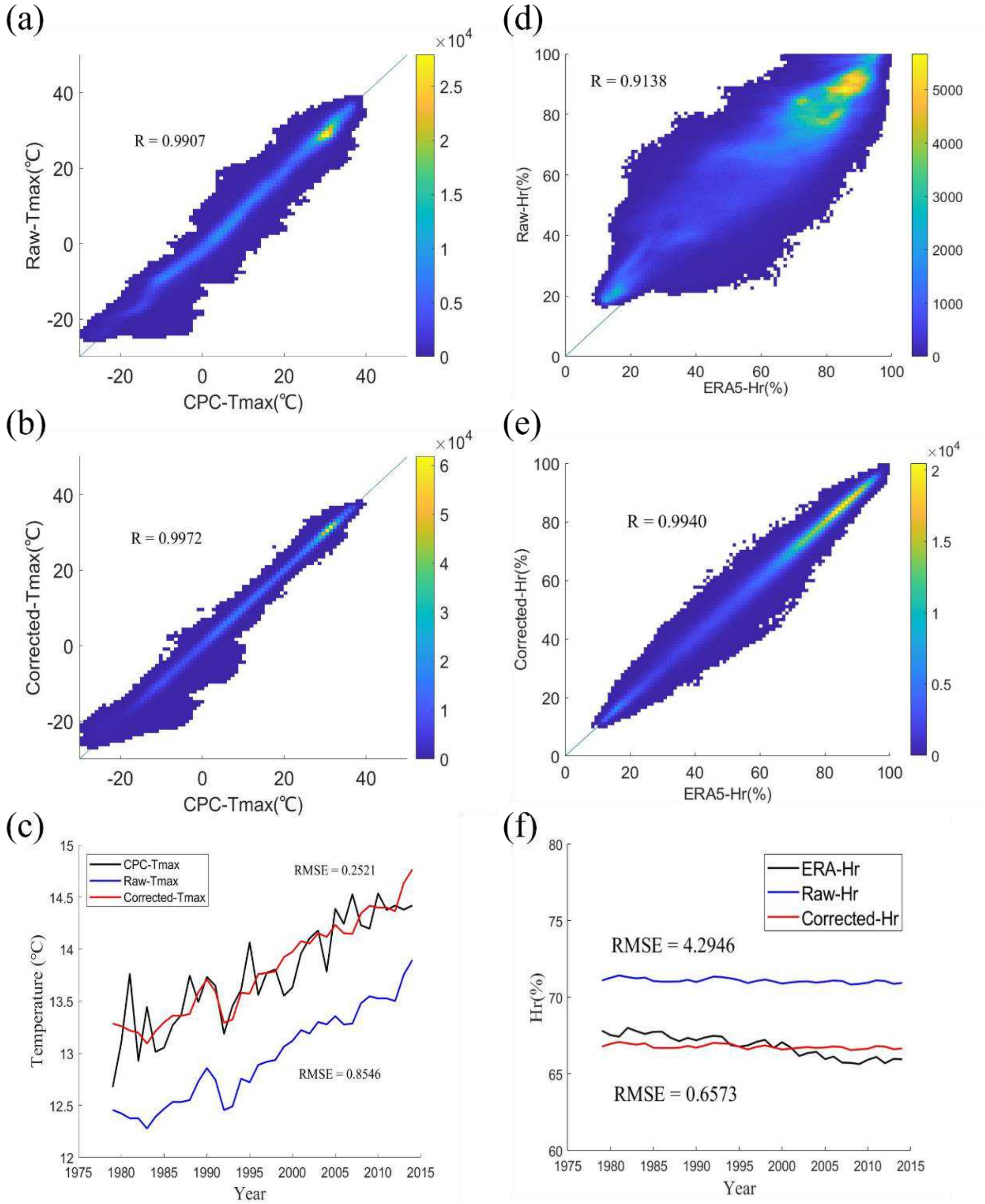

Figure 2. Bias correction performance of annual average T_{max} form multi-model ensemble for 1979-2014 over global land areas. (a) Bin scatter of the raw T_{max} and observed Tmax for all global land pixels. (b) is corrected T_{max}. (c) change in global land T_{max} for 1979-2014. (d-f) is same for H_r.

We divided the future period into three sub-periods according to the IPCC AR6 (near term (2021-2040), mid-term (2041-2060), long term (2081-2100)) and use observed data and corrected CMIP6 data to calculate the historical and future T_w. Figure 3 showed the spatial feature and global average change of T_w for historical and different scenarios future period. Then we calculated the T_w changes relative to the baseline period (1979-2014) for different periods. T_w has an increasing trend in almost all land pixels under four future scenarios. The spatial distribution of T_w increases in the three scenarios with higher emissions (SSP2-4.5, SPP3-7.0, SSP5-8.5) is similar, with the greatest warming in northern North America, central Africa, the Qinghai-Tibet Plateau, and the Malay Archipelago than the remaining regions. In the near term, there is no significant difference in increase between the four future scenarios, the warming in all scenarios is around 1.8°C. But for the long term, the SSP3-7.0 and SSP5-8.5 scenarios have very significant warming, with most of the global land pixels warming above 5°C and some regions will warm by more than 7°C.

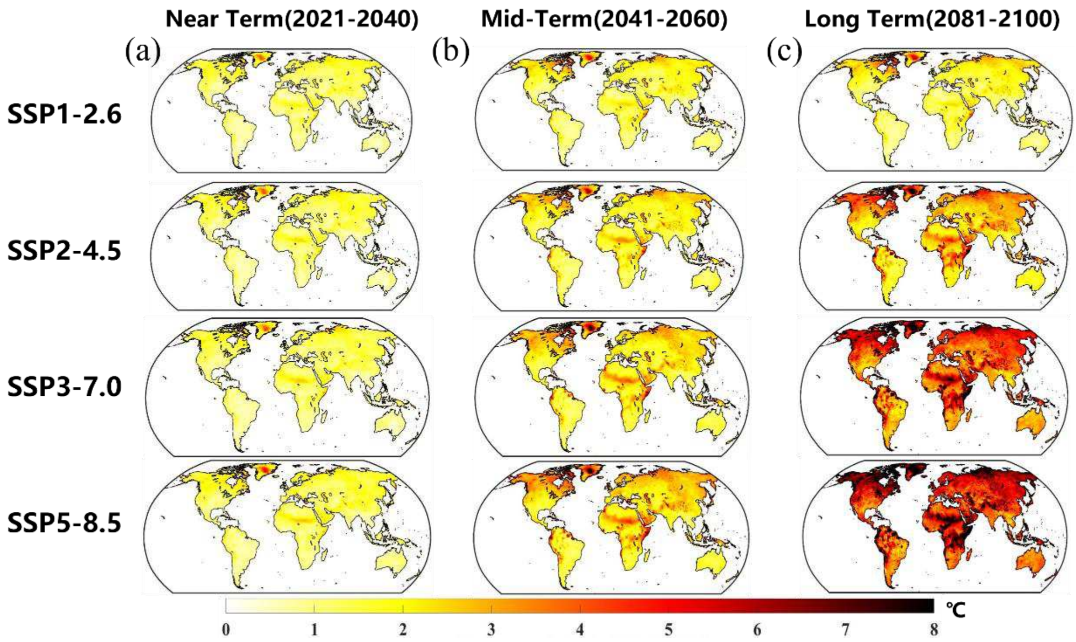

Figure 3. Spatial features of T_w using 1979-2014 baseline for diverse future scenarios at (a) Near Term (2021-2040), (b) Mid-Term (2041-2060) and (c) Long Term (2081-2100).

We then calculated the full time series of the global average T_w and probability density function (PDF). According to Figure 4, the four future scenarios do not differ significantly in warming magnitudes until 2050. After 2050, the warming in the SSP1-2.6 scenario almost stops and remains at 1.8°C due to lower emission levels and mitigation measures, while the other three scenarios show continuous warming, with the SSP5-8.5 scenario showing the fastest warming, reaching 6.7°C at the end of 21st century. The same conclusion can be drawn from the probability density plot, where both the mean and variance are smaller for scenario SSP1-2.6, implying that the warming in this scenario is smaller and closer to historical values. The higher emissions scenarios have larger means and variances, implying higher warming level.

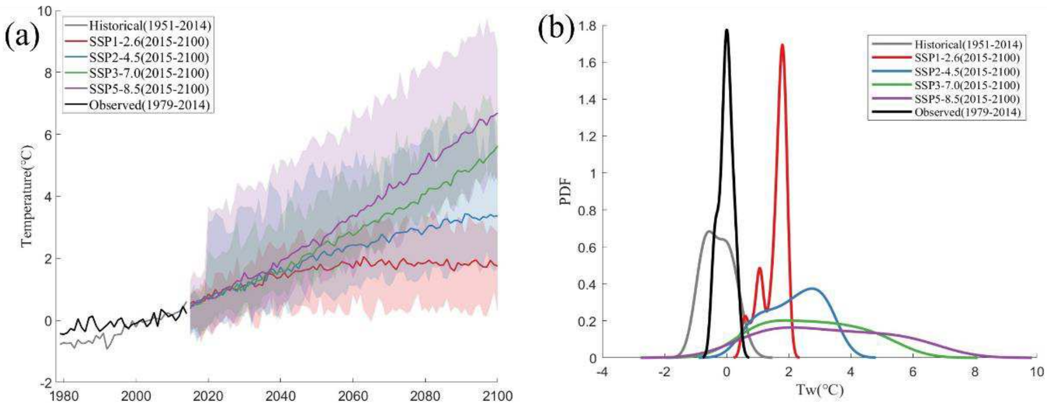

Figure 4 (a) Time series and probability density function (b) Probability density function of global annual average T_w relative to 1979-2014. Shading areas denote the interquartile ensemble spread, i.e. the range between the 25th and 75th percentiles of the model ensemble, representing the inter-model uncertainty.

We divided the global land area into 46 sub-regions based on the IPCC AR6 and analyzed 44 non-polar sub-regions. Figure 5 shows the T_w of history period and four future scenarios over different regions. In the historical and near term, the average T_w is below 32°C in all regions of the world, and there was little difference in warming between sub-regions. In the mid-term, the average T_w of CAR and SEA is close to 35°C, meaning that in some areas T_w has already above 35°C, which can pose a serious threat to human body. In the long term, the average T_w of CAR, SEA, WAF, CAF, NEAF, SEAF and SEA is close or more than 35°C, meaning that the equatorial region will face serious threats in the future. By the end of 21st century, the GIC, NEN, CAR, NEAF and SEAF sub-regions will have warmed much more than the global average, approaching 9°C in scenario SSP5-8.5. This puts a huge strain on the adaptive capacity of the local population. Although the latitude of NWN, NEN and GIC is high and T_w is still safe for human in the future, the significant increase of T_w in these regions may pose other environmental problems that will also require attention in the future.

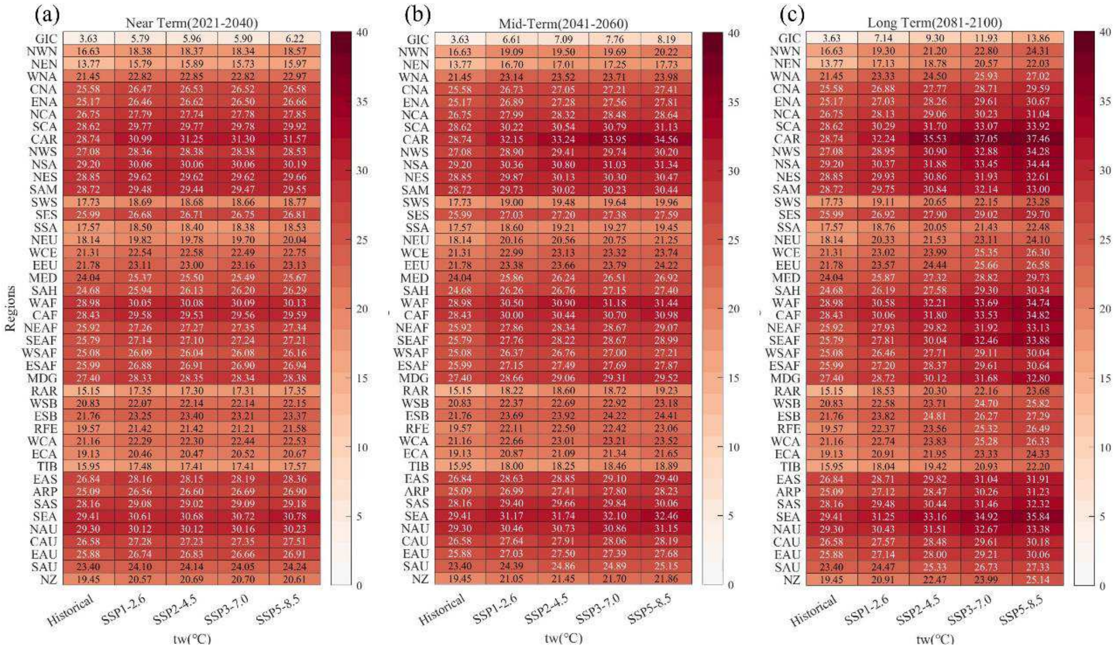

Figure 5 Heatmap of T_w for history period and four future scenarios in different sub-regions. (a) Near Term (2021-2040). (b) Mid-Term (2041-2060). (c) Long Term (2080-2100).

3.2 Projected Changes in Population Exposure

Since T_w is a measure of environmental heat stress on humans, it is necessary to combine population data to assess the impact of T_w rise on humans. In the historical period, only a few land pixels of T_w occasionally exceeded 35°C. Figure 6(a-d) shows the spatial distribution of the number of days in a year when T_w exceeds 35°C for different emission scenarios at the end of 21st century. In scenarios SSP1-2.6 and SSP2-4.5, the exposed areas at the end of 21st century are very similar to the current ones due to the low level of warming, and only a few pixels such as CAR, WAF and SEA have some exposure. In scenarios SSP3-7.0 and SSP5-8.5, exposure occurs in regions near the equator, in the Caribbean, and in southeastern China. The area exposed under the scenario SSP3-7.0 is small, but the excessive population makes the exposure under this scenario almost equal to scenario SSP5-8.5 which has the higher temperature. In addition, the area of exposure in the Indian region is not large (308 and 642 thousand square kilometer under scenario SSP3-7.0 and SSP5-8.5, respectively), but the exposure remains large due to the extremely high population density in the region.

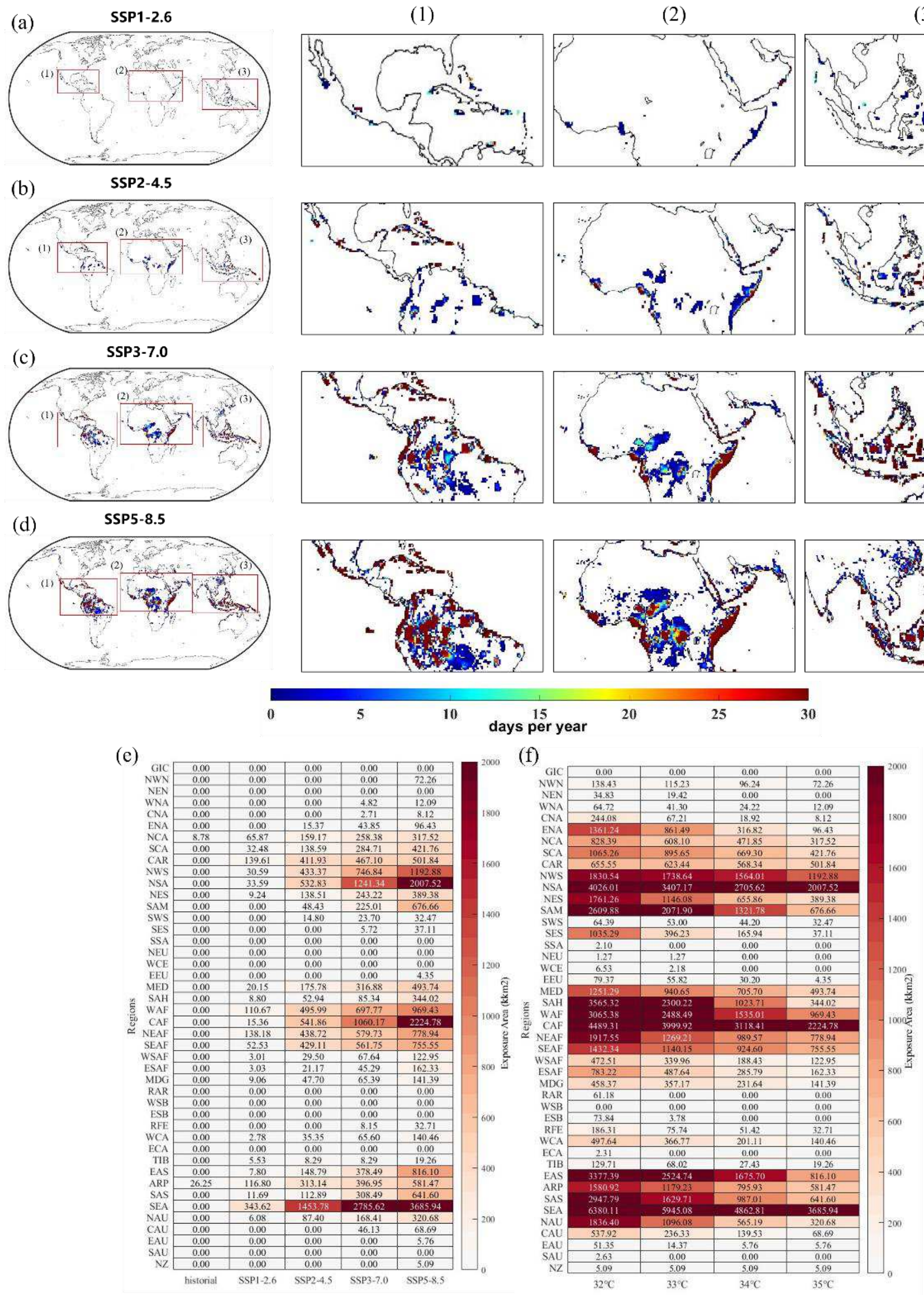

Figure 6. Spatiotemporal features of future population exposure and exposure area. (a-d) Spatial distribution of exposure under four scenarios (SSP1-2.6, SSP2-4.5, SSP3-

7.0, SSP5-8.5) in the long term, respectively. (1-3) is an enlargement of focus area of (a-d). (e) Sub-regions exposure area for each scenario at 35°C threshold. (b) Sub-region exposure area exceeded different thresholds under scenario SSP5-8.5.

We also analyzed the time series of population exposure (Figure 7). Population exposure is low for each scenario until 2050, and after 2050 there is a slow increase in exposure in the SSP2-4.5 scenario and a rapid increase in exposure in SSP5-8.5 and SSP3-7.0. In the middle and late stages of scenario SSP1-2.6, population exposure tends to decrease as T_w stops increase and the population decreases, but in the SSP2-4.5 and SSP5-8.5 scenarios, the increase in T_w offsets the decrease in population and the population exposure remains on an upward trend. Due to the rapid population growth in the scenario SSP3-7.0 and the strong temperature rise in the scenario SSP5-8.5, the population exposure in both scenarios increased rapidly, reaching 10^5 million person-day at the end of 21^{st} century.

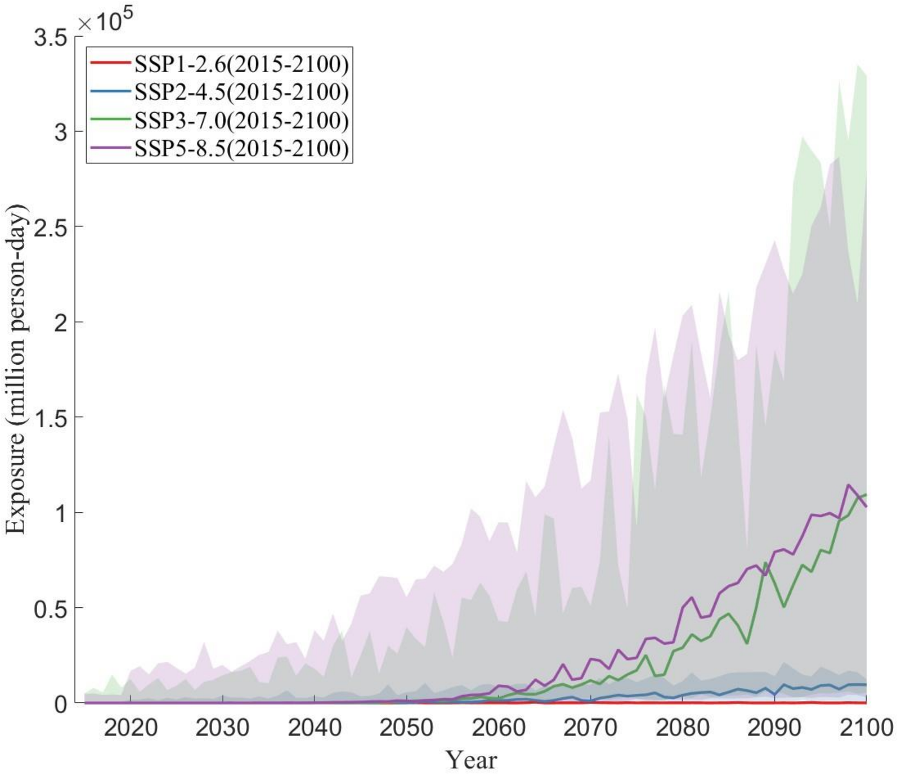

Figure 7. Time series of future global population exposure to CHHE under four scenarios (SSP1-2.6, SSP2-4.5, SSP3-7.0, SSP5-8.5). Shading areas denote the interquartile ensemble spread, i.e. the range between the 25th and 75th percentiles of the model ensemble, representing the inter-model uncertainty.

Furthermore, we examined the number of days of exposure under other thresholds in the scenario SSP3-7.0 and SSP5-8.5 (Figure 8). As the threshold decreases, the exposed area gradually expands to both sides of the equator. When T_w threshold decreases 3°C to 32°C, exposure increases ten-fold in subregion EAS and ENA, where increase faster than other regions at the same latitude (Figure 9(b)). It may be due to the high urbanization rate and the significant urban heat island effect in these areas.

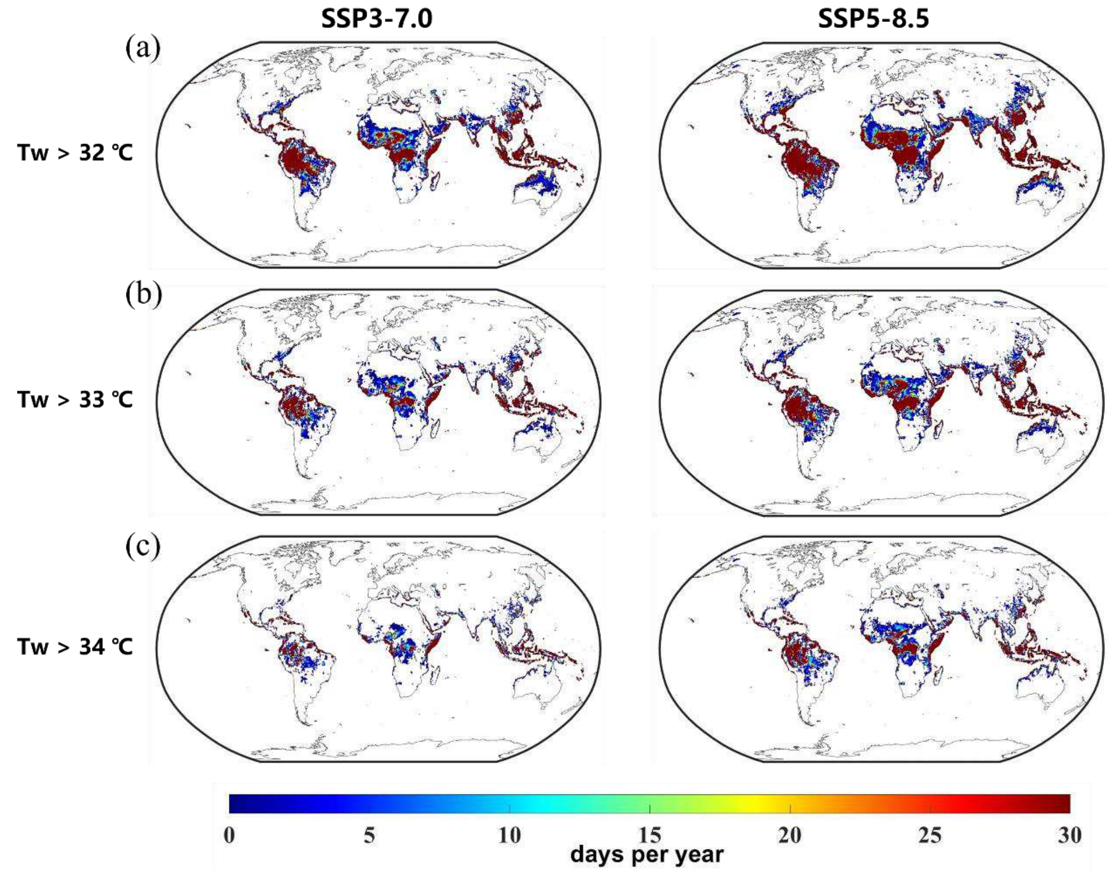

Figure 8. Spatial distribution of exposure at different thresholds of T_w at the end of 21st century under scenario SSP3-7.0 and SSP5-8.5. (a-c) represent 32℃, 33℃ and 34℃ thresholds, respectively.

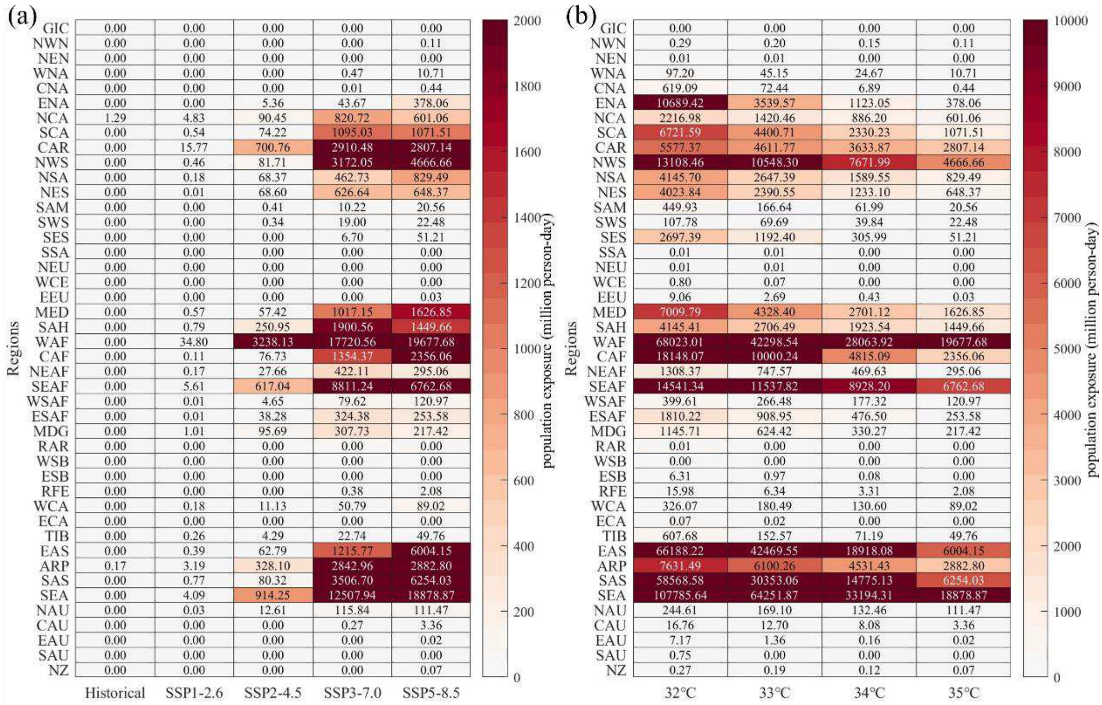

Figure 9 (a) Sub-regions population exposure for each scenario at 35°C threshold. (b) Sub-region population exposure exceeded different thresholds under scenario SSP5-8.5.

3.3 Contributions of population and climate change to increased exposure

To better understand how heatwaves affect humans and to develop mitigation measures, we analyzed the contribution of future climate and population changes to exposure changes globally and in 44 sub-regions. Population changes accounts for about 20% in 2020 and decreases over time, converging to 0 after 2050 (Fig. 10). In the long term, the contribution of each factor is relatively stable under scenario SSP1-2.6, with climate change accounting for about 80% and the population-climate interactions for 20%. In scenarios SSP2-4.5 and SSP3-7.0, the proportion of interactions gradually increases and approaches 50% at the end of 21st century, indirectly indicating a further increase in the relative role of population change. In scenario SSP5-8.5, the proportion of interactions increases and then decreases due to strong warming effects, with an extreme value in 2060 and a share of about 10% at the end of 21st century. These results suggest that climate change dominates future increases in population exposure, particularly in Africa, and the impact of population growth cannot be ignored.

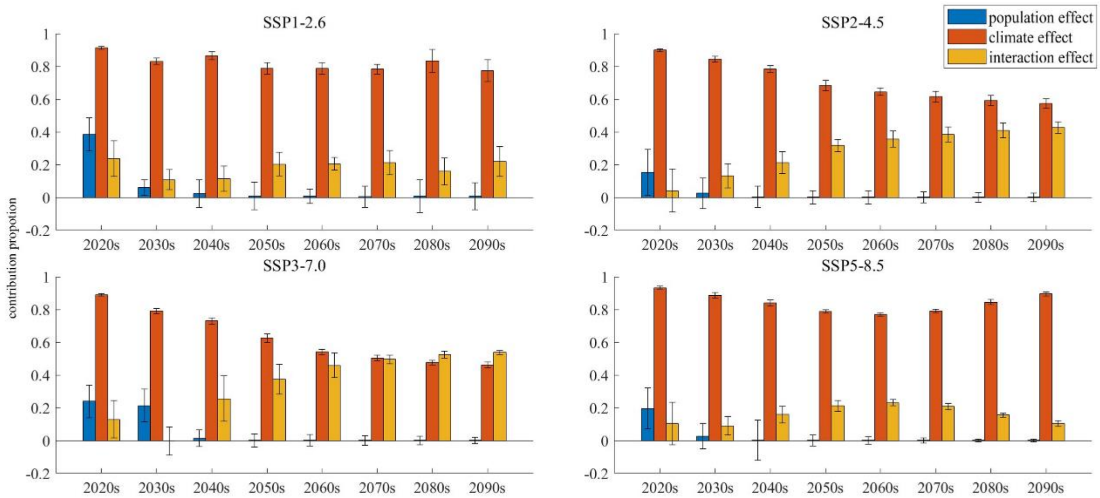

Figure 10. Contributions of climate, population and population-climate interaction effects to change in total population exposure in four scenarios. (a-d) Global average contribution proportion for scenarios of SSP1-2.6, SSP2-4.5, SSP3-7.0, SSP5-8.5, respectively.

The contribution of each factor was calculated for the scenarios, considering the variability between regions (Fig. 11). Because not every sub-region has exposure and attribution analysis for a smaller number of exposure sub-regions would have a larger error, we only considered sub-regions with more than 100 exposure pixels. In the scenario SSP3-7.0, the African region has a rapid population increase, so the interaction proportion is significantly higher in the WAF, CAF, NEAF and SEAF sub-regions than in the other regions. In the exposed areas, only EAS has some population decrease, so the interaction proportion is negative. In scenario SSP5-8.5, the EAS, SAS, SEA and Americas all experience population declines at the end of 21st century, so the interaction proportions for this region are all negative. There is a small amount of population growth in Africa, so the interaction ratio is positive, but less than the scenario SSP3-7.0. According to Figure 11, WAF, CAF, NEAF and SEAF sub-regions will experience higher warming than the global average, and their populations will grow rapidly with lack of adaption and cooling infrastructures.

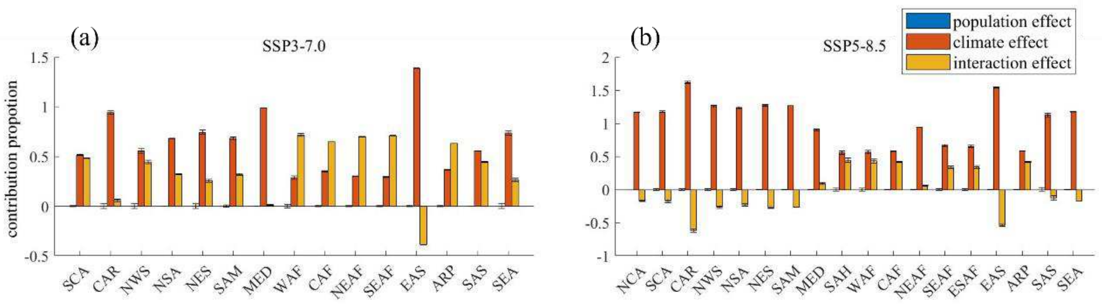

Figure 11. Proportion of contribution of population effect, climate effect and interaction effect to population in each sub-region at the end of 21st century under scenario (a) SSP3-7.0 and (b) SSP5-8.5, respectively.

3.4 Discussion

In this study, we first examined projected changes in the future CHHE. Our result show that global T_w will increase significantly in the future due to climate change. This is consistent with pervious studied in Africa and China (*Fotso-Nguemo et al.*, 2023; *H. Chen et al.*, 2022). Even in the scenario SSP1-2.6 with minimum emissions and mitigation measures, where anthropogenic greenhouse gas emissions are significantly reduced to reach carbon neutrality, there is a 1.8°C warming in T_w, which would result in T_w exceeding 32°C in the CAR SEA region, and outdoor work in summer would be affected. In contrast, under scenario SSP5-8.5 global average warming of T_w would reach 6.7°C, with some areas approaching 9°C. Large areas near the equator would have T_w exceeding 35°, and without cooling facilities, prolonged outdoor activities would become unfeasible.

Under scenarios SSP3-7.0 and SSP5-8.5, the region near the equator will have a large area exposed to T_w>35°, while the scenarios SSP2-4.5 and SSP1-2.6 are safer with few area of exposure. Presumably high forest cover and high relative humidity in areas such as SEA NSA and CAF, resulting in a high heat index. On the other hand, the African region is experiencing higher warming, so the heat stress index is also rising faster. In the future, much of Africa is expected to still lack adequate adaptation and mitigation measures, especially considering the rapid population growth (*Asefi-Najafabady et al.*, 2018; *Weber et al.*, 2018). Without the establishment of effective cooling facilities in these areas, heatwave and humidity extremes could lead to severe heat stroke and fatalities (*Thiery et al.*, 2021).

In the European heatwave of 2003, a 32°C T_w already caused the deaths of elderly people and children (*Coffel et al.*, 2018; *Fouillet et al.*, 2008). To explore potential future risk exposure and impact on outdoor labor, we calculated exposure under different thresholds for scenario SSP3-7.0 and SSP5-8.5. At the 32°C threshold, there is a several-fold increase in exposure in both equatorial regions. In addition, the

EAS and ENA sub-regions have much higher increases in exposure than other regions at the same latitude, but these two sub-regions are more developed in the future, are better able to develop continuous mitigation policies and have more cooling facilities, and the impact of high temperatures on human health will be less than in low-income areas. However, heatwave events can affect outdoor work and increase stress on power systems. In these areas, future studies should pay more attention to the impact of heatwaves on infrastructure and the economy (*Rajeev and Mishra*, 2022; *Yin et al.*, 2023).

Climate change, population change, and their interaction effect are main factors causing increased exposure (*Coffel et al.*, 2018; *Raymond et al.*, 2020). When we calculated the relative contribution of population, we used historical meteorological data, which rarely exceeded the threshold, making the contribution of population change almost zero (*Chen et al.*, 2022; *Coffel et al.*, 2018). Population exposure in 2020s is small but its uncertainty range is large that means population exposure has large relative bias in 2020s. The large uncertainty make sum of three contribution proportion exceed 1. The portion above 1 represents the effect of data uncertainty. As population exposure increase, the influence of uncertainties decreases, the sum of three factors' contribution proportion is close to 1. The proportion of population climate interactions indirectly reflects the impact of population change when the change of population exposure is large and the uncertainties of data cannot influence the result too much. Climate change dominates the increase in exposure at all future times in all scenarios. As populations in Africa and South Asia will continue to increase in the future, the contribution of population-climate interactions in these regions is greater than in other regions, exceeding 50% in scenario SSP3-7.0. In scenario SSP5-8.5, the population decrease in many sub-regions, leading negative contribution of interaction. Only several Africa sub-region which have much population having small positive contribution of interaction (*Coffel et al.*, 2018). There is an urgent need to reduce anthropogenic greenhouse gas emissions and reduce the extent of global warming on a global scale. In developing countries in Africa and SEA, mitigation policies, universal access to cooling facilities and controlled population growth should be put in place to help reduce losses in the areas most affected by extreme heatwave events (*Fotso-Nguemo et al.*, 2023; *Tuholske et al.*, 2021).

Recently, some studies started to focus on the effects of radiation on human health. Previous indicated solar radiation can reduce human endurance exercise capacity (*Otani, Kaya, Tamaki, Watson*, & *Maughan*, 2016). Human's head directly expose to solar radiation outdoor, and human's brain is vulnerable to the environmental conditions. Exposure to direct solar radiation at lower temperatures may also be hazardous to human health (*Piil et al.*, 2020). There is longer hours of sunlight and stronger radiation in equatorial regions and peoples there may face the greater threat in the future.

Although we used bias correction and multi-model ensemble data to simulate future CHHE, uncertainty of future data is still inevitable. Uncertainties of T_w change and population increase as time. However, with population exposure increase as time, uncertainties of contribution decrease. Because the larger ΔCE bring larger ΔE, and the value of contribution is related to ΔCE/ΔE, the variance between the different model will be smaller than single factor. Scenario SSP1-2.6 has largest uncertainty because of smallest population exposure. Scenario SSP3-7.0 and SSP5-8.5 have very small uncertainties at the end of century. Besides the model uncertainty mentioned above, observed data, resample method and bias correction method we used may also have uncertainties. Recently, several studies used machine learning method to generate high resolution climate data, these new methods provide a new way to improve the accuracy of future projections (*Anderson & Lucas*, 2018; *Yuval & O'Gorman*, 2020).

4 Conclusions

In this study, we investigated the changes of compound heatwave and humidity extremes in global scale, using T_w from CMIP6 models under historical and different future scenarios including SSP1-2.6, SSP2-4.5, SSP3-7.0 and SSP5-8.5. Furthermore, we explore the characteristics of population exposure change and attribution of exposure change. The main conclusions are down as follows.

(1) The global T_w will increase significantly in the future. The warming under four scenarios (SSP1-2.6, SSP2-4.5, SSP3-7.0, SSP5-8.5) is 1.79°C, 3.37°C, 5.46°C, 6.69°C, respectively. Large areas near the equator would have T_w exceeding 35°.

(2) Population exposure in the equatorial region will increase significantly under high emissions scenarios, reaching 10^5 million person-day by the end of 21st century.

And the rate of exposure increase in southeastern American and southeastern China is faster than other regions.

(3) Climate change dominates the increase in exposure at all future times in all scenarios. At the end of 21st century, climate change dominates the increase in exposure in all scenarios, with a proportion of 80%, 60%, 45%, and 90% under SSP1-2.6, SSP2-4.5, SSP3-7.0, and SSP5-8.5 scenarios, respectively.

Author contributions

All authors contributed to the study conception and design. The idea of this study was proposed by DS. Data was collected by TW. YW, JX, GW, QZ, SH and YZ analyzed the data and YW wrote the initial manuscript. All the authors have read the manuscript and accepted the author's agreement.

Funding

This research was funded by the National Natural Science Foundation of China (No.52179023) and Hubei Provincial Natural Science Foundation of China (No. 2023AFA081 and 2023BCA003).

Availability of data and material

CMIP6 data is available at https://esgf-node.llnl.gov/search/cmip6/. Climate Prediction Center data can be downloaded from https://psl.noaa.gov/data/gridded/data.cpc.globaltemp.html. ERA5 data is available at https://cds.climate.copernicus.eu/cdsapp#!/dataset/reanalysis-era5-land. Population data is available at https://iiasa.ac.at/models-tools-data/ssp.

Declarations

Conflict of interest The authors declare that they have no competing interests.

References

Alexander, L. V., et al. (2006), Global observed changes in daily climate extremes of temperature and precipitation, *Journal of Geophysical Research*, *111*(D5). https://doi.org/10.1029/2005JD006290

Anderson, G. J., & Lucas, D. D. (2018). Machine Learning Predictions of a Multiresolution Climate Model Ensemble. *Geophysical Research Letters, 45*(9), 4273-4280. https://doi.org/10.1029/2018GL077049

Asefi-Najafabady, S., K. L. Vandecar, A. Seimon, P. Lawrence, and D. Lawrence (2018), Climate change, population, and poverty: vulnerability and exposure to heat stress in countries bordering the Great Lakes of Africa, *Climatic Change*, *148*(4), 561-573. https://doi.org/10.1007/s10584-018-2211-5

Ballester, J., Quijal-Zamorano, M., Méndez Turrubiates, R.F. *et al.* Heat-related mortality in Europe during the summer of 2022. *Nat Med* **29**, 1857–1866 (2023). https://doi.org/10.1038/s41591-023-02419-z

Bardon, L. R., B. A. Ward, S. Dutkiewicz, and B. B. Cael (2021), Testing the Skill of a Species Distribution Model Using a 21st Century Virtual Ecosystem, *Geophysical Research Letters*, *48*(22), e2021GL093455. https://doi.org/10.1029/2021GL093455

Buzan, J. R., K. Oleson, and M. Huber (2015), Implementation and comparison of a suite of heat stress metrics within the Community Land Model version 4.5, *Geoscientific Model Development*, *8*(2), 151-170. https://doi.org/10.5194/gmd-8-151-2015

Byrne, M. P., and P. A. O'Gorman (2018), Trends in continental temperature and humidity directly linked to ocean warming, *Proceedings of the National Academy of Sciences*, *115*(19), 4863-4868. https://doi.org/10.1073/pnas.1722312115

Cannon, A. J., S. R. Sobie, and T. Q. Murdock (2015), Bias Correction of GCM Precipitation by Quantile Mapping: How Well Do Methods Preserve Changes in Quantiles and Extremes?, *Journal of Climate*, *28*(17), 6938-6959. https://doi.org/10.1175/JCLI-D-14-00754.1

Chen, H., and J. Sun (2021), Significant Increase of the Global Population Exposure to Increased Precipitation Extremes in the Future, *Earth's Future*, *9*(9), e2020EF001941. https://doi.org/10.1029/2020EF001941

Chen, H., J. Sun, W. Lin, and H. Xu (2020), Comparison of CMIP6 and CMIP5 models in simulating climate extremes, *Science Bulletin*, *65*. https://doi.org/10.1016/j.scib.2020.05.015

Chen, H., W. He, J. Sun, and L. Chen (2022), Increases of extreme heat-humidity days endanger future populations living in China, *Environmental Research Letters*, *17*(6). https://doi.org/10.1088/1748-9326/ac69fc

Chen, J., R. Arsenault, F. P. Brissette, and S. Zhang (2021), Climate Change Impact Studies: Should We Bias Correct Climate Model Outputs or Post-Process Impact Model Outputs?, *Water Resources Research*, *57*(5), e2020WR028638. https://doi.org/10.1029/2020WR028638

Coffel, E. D., R. M. Horton, and A. de Sherbinin (2018), Temperature and humidity based projections of a rapid rise in global heat stress exposure during the 21(st) century, Environmental Research Letters, 13(1). https://doi.org/10.1088/1748-9326/aaa00e

Cook, B. I., J. S. Mankin, K. Marvel, A. P. Williams, J. E. Smerdon, and K. J. Anchukaitis (2020), Twenty-First Century Drought Projections in the CMIP6 Forcing Scenarios, *Earth's Future*, *8*(6), e2019EF001461. https://doi.org/10.1029/2019EF001461

Davies-Jones, R. (2008), An Efficient and Accurate Method for Computing the Wet-Bulb Temperature along Pseudoadiabats, *Monthly Weather Review*, *136*(7), 2764-2785. https://doi.org/10.1175/2007MWR2224.1

Diffenbaugh, N. S., J. S. Pal, F. Giorgi, and X. Gao (2007), Heat stress intensification in the Mediterranean climate change hotspot, *Geophysical Research Letters*, *34*(11). https://doi.org/10.1029/2007GL030000

Dunne, J. P., R. J. Stouffer, and J. G. John (2013), Reductions in labour capacity from heat stress under climate warming, *Nature Climate Change*, *3*(6), 563-566.

Epstein, Y., and D. S. Moran (2006), Thermal Comfort and the Heat Stress Indices, *Industrial Health*, *44*(3), 388-398. https://doi.org/10.1038/nclimate1827

Feng, Y., F. Sun, W. Liu, J. Chen, H. Wang, Q. Guo, Y. Wang, Q. Zhang, and Y.-F. Sang (2022), Changes in compound hot and dry day and population exposure across China under climate change, *International Journal of Climatology*, *42*(5), 2935-2949. https://doi.org/10.1002/joc.7399

Fischer, E. M., and C. Schär (2010), Consistent geographical patterns of changes in high-impact European heatwaves, *Nature Geoscience*, *3*(6), 398-403. https://doi.org/10.1038/ngeo866

Fotso-Nguemo, T. C., T. Weber, A. Diedhiou, S. Chouto, D. A. Vondou, D. Rechid, and D. Jacob (2023), Projected Impact of Increased Global Warming on Heat Stress and Exposed Population Over Africa, *Earth's Future*, *11*(1), e2022EF003268. https://doi.org/10.1029/2022EF003268

Fouillet, A., et al. (2008), Has the impact of heat waves on mortality changed in France since the European heat wave of summer 2003? A study of the 2006 heat wave, *International Journal of Epidemiology*, *37*(2), 309-317. https://doi.org/10.1093/ije/dym253

Gu, L., Chen, J., Yin, J., Slater, L. J., Wang, H. M., Guo, Q., . . . Zhao, T. (2022). Global Increases in Compound Flood‐Hot Extreme Hazards Under Climate Warming. *Geophysical Research Letters, 49*(8). https://doi.org/10.1029/2022GL097726

Haines, A., R. S. Kovats, D. Campbell-Lendrum, and C. Corvalan (2006), Climate change and human health: Impacts, vulnerability and public health, *Public Health*, *120*(7), 585-596. https://doi.org/10.1016/j.puhe.2006.01.002

Huang, X., Song, J., Wang, C., Chui, T. F. M., & Chan, P. W. (2021). The synergistic effect of urban heat and moisture islands in a compact high-rise city. *Building and Environment, 205*. https://doi.org/10.1016/j.buildenv.2021.108274

Im, E.-S., J. S. Pal, and E. A. B. Eltahir (2017), Deadly heat waves projected in the densely populated agricultural regions of South Asia, *Science Advances*, *3*(8), e1603322. https://doi.org/10.1126/sciadv.1603322

IPCC (2021), Climate change 2021: The physical science bases. Contribution of working group i to the sixth assessment report of the intergovernmental panel on climate change. https://www.ipcc.ch/report/ar6/wg1/

Jones, B., B. C. O'Neill, L. McDaniel, S. McGinnis, L. O. Mearns, and C. Tebaldi (2015), Future population exposure to US heat extremes, *Nature Climate Change*, *5*(7), 652-655. https://doi.org/10.1038/nclimate2631

Jun, M., R. Knutti, and D. W. Nychka (2008), Spatial Analysis to Quantify Numerical Model Bias and Dependence, Journal of the American Statistical Association, 103(483), 934-947. https://doi.org/10.1198/016214507000001265

Kc, S., and W. Lutz (2017), The human core of the shared socioeconomic pathways: Population scenarios by age, sex and level of education for all countries to 2100, *Global Environmental Change*, *42*, 181-192. https://doi.org/10.1016/j.gloenvcha.2014.06.004

Kurz, W. A., C. C. Dymond, G. Stinson, G. J. Rampley, E. T. Neilson, A. L. Carroll, T. Ebata, and L. Safranyik (2008), Mountain pine beetle and forest carbon feedback to climate change, *Nature*, *452*(7190), 987-990. https://doi.org/10.1038/nature06777

Lesk, C., E. Coffel, A. W. D'Amato, K. Dodds, and R. Horton (2017), Threats to North American forests from southern pine beetle with warming winters, *Nature Climate Change*, *7*(10), 713-717. https://doi.org/10.1038/nclimate3375

Li, D., J. Yuan, and R. E. Kopp (2020), Escalating global exposure to compound heat-humidity extremes with warming, *Environmental Research Letters*, *15*(6). https://doi.org/10.1088/1748-9326/ab7d04

Li, X. X. (2020). Heat wave trends in Southeast Asia during 1979-2018: The impact of humidity. *Sci Total Environ, 721*, 137664. https://doi.org/10.1016/j.scitotenv.2020.137664

Liang, C., G. Zheng, N. Zhu, Z. Tian, S. Lu, and Y. Chen (2011), A new environmental heat stress index for indoor hot and humid environments based on Cox regression, *Building and Environment*, *46*(12), 2472-2479. https://doi.org/10.1016/j.buildenv.2011.06.013

Liu, M., Y. Yin, X. Wang, X. Ma, Y. Chen, and W. Chen (2022), More frequent, long-lasting, extreme and postponed compound drought and hot events in eastern China, Journal of Hydrology, 614. https://doi.org/10.1016/j.jhydrol.2022.128499

Maraun, D. (2013), Bias Correction, Quantile Mapping, and Downscaling: Revisiting the Inflation Issue, *Journal of Climate*, *26*(6), 2137-2143. https://doi.org/10.1175/JCLI-D-12-00821.1

Maurer, E. P., H. G. Hidalgo, T. Das, M. D. Dettinger, and D. R. Cayan (2010), The utility of daily large-scale climate data in the assessment of climate change impacts on daily streamflow in California, *Hydrology and Earth System Sciences*, *14*(6), 1125-1138. https://doi.org/10.5194/hess-14-1125-2010

Mukherjee, S., and A. K. Mishra (2021), Increase in Compound Drought and Heatwaves in a Warming World, *Geophysical Research Letters*, *48*(1). https://doi.org/10.1029/2020GL090617

Nashwan, M. S., S. Shahid, and E.-S. Chung (2019), Development of high-resolution daily gridded temperature datasets for the central north region of Egypt, *Scientific Data*, *6*(1), 138. https://doi.org/10.1038/s41597-019-0144-0

O'Neill, B. C., et al. (2016), The Scenario Model Intercomparison Project (ScenarioMIP) for CMIP6, Geoscientific Model Development, 9(9), 3461-3482. https://doi.org/10.5194/gmd-9-3461-2016

Otani, H., Kaya, M., Tamaki, A., Watson, P., & Maughan, R. J. (2016). Effects of solar radiation on endurance exercise capacity in a hot environment. *Eur J Appl Physiol, 116*(4), 769-779. https://doi.org/10.1007/s00421-016-3335-9

Pal, J. S., and E. A. B. Eltahir (2016), Future temperature in southwest Asia projected to exceed a threshold for human adaptability, *Nature Climate Change*, *6*(2), 197-200. https://doi.org/10.1038/nclimate2833

Petkova, E. P., R. M. Horton, D. A. Bader, and P. L. Kinney (2013), Projected heat-related mortality in the U.S. urban northeast, *International Journal of Environmental Research and Public Health*, *10*(12), 6734-6747. https://doi.org/10.3390/ijerph10126734

Piil, J. F., Christiansen, L., Morris, N. B., Mikkelsen, C. J., Ioannou, L. G., Flouris, A. D., . . . Nybo, L. (2020). Direct exposure of the head to solar heat radiation impairs motor-cognitive performance. *Sci Rep, 10*(1), 7812. https://doi.org/10.1038/s41598-020-64768-w

Rajeev, A., and V. Mishra (2022), Observational evidence of increasing compound tropical cyclone - moist heat extremes in India, *Earth's Future*, 10(12). https://doi.org/10.1029/2022EF002992

Raymond, C., T. Matthews, and R. M. Horton (2020), The emergence of heat and humidity too severe for human tolerance, *Science Advances*, *6*(19), eaaw1838. https:doi.org/10.1126/sciadv.aaw1838

Riahi, K., et al. (2017), The Shared Socioeconomic Pathways and their energy, land use, and greenhouse gas emissions implications: An overview, *Global Environmental Change*, *42*, 153-168. https://doi.org/10.1016/j.gloenvcha.2016.05.009

Ridder, N. N., A. J. Pitman, S. Westra, A. Ukkola, H. X. Do, M. Bador, A. L. Hirsch, J. P. Evans, A. Di Luca, and J. Zscheischler (2020), Global hotspots for the occurrence of compound events, *Nature Communications*, *11*(1), 5956. https://doi.org/10.1038/s41467-020-19639-3

Rogers, C. D. W., M. Ting, C. Li, K. Kornhuber, E. D. Coffel, R. M. Horton, C. Raymond, and D. Singh (2021), Recent Increases in Exposure to Extreme Humid‐Heat Events Disproportionately Affect Populated Regions, *Geophysical Research Letters*, *48*(19). https://doi.org/10.1029/2021GL094183

Schär, C. (2016), The worst heat waves to come, *Nature Climate Change*, *6*(2), 128-129. https://doi.org/10.1038/nclimate2864

Sherwood, S. C., and M. Huber (2010), An adaptability limit to climate change due to heat stress, *Proceedings of the National Academy of Sciences*, *107*(21), 9552-9555. https://doi.org/10.1073/pnas.0913352107

Shi, L., Luo, Z., Matthews, W., Wang, Z., Li, Y., & Liu, J. (2019). Impacts of urban microclimate on summertime sensible and latent energy demand for cooling in residential buildings of Hong Kong. *Energy, 189*. https://doi.org/10.1016/j.energy.2019.116208

Tang, G., M. P. Clark, and S. M. Papalexiou (2021), SC-Earth: A Station-Based Serially Complete Earth Dataset from 1950 to 2019, *Journal of Climate*, *34*(16), 6493-6511. https://doi.org/10.1175/JCLI-D-21-0067.1

Tarek, M., F. Brissette, and R. Arsenault (2021), Uncertainty of gridded precipitation and temperature reference datasets in climate change impact studies, *Hydrology and Earth System Sciences*, *25*(6), 3331-3350. https://doi.org/10.5194/hess-25-3331-2021

Thiery, W., et al. (2021), Intergenerational inequities in exposure to climate extremes, *Science*, *374*(6564), 158-160. https://doi.org/10.1126/science.abi7339

Thrasher, B., E. P. Maurer, C. McKellar, and P. B. Duffy (2012), Technical Note: Bias correcting climate model simulated daily temperature extremes with quantile mapping, *Hydrology and Earth System Sciences*, *16*(9), 3309-3314. https://doi.org/10.5194/hess-16-3309-2012

Tripathy, K. P., S. Mukherjee, A. K. Mishra, M. E. Mann, and A. P. Williams (2023), Climate change will accelerate the high-end risk of compound drought and heatwave events, *Proceedings of the National Academy of Sciences*, 120(28), e2219825120. https://doi.org/10.1073/pnas.2219825120

Tuholske, C., K. Caylor, C. Funk, A. Verdin, S. Sweeney, K. Grace, P. Peterson, and T. Evans (2021), Global urban population exposure to extreme heat, *Proceedings of the National Academy of Sciences*, *118*(41). https://doi.org/10.1073/pnas.2024792118

Ullah, S., Q. You, D. Chen, D. A. Sachindra, A. AghaKouchak, S. Kang, M. Li, P. Zhai, and W. Ullah (2022), Future Population Exposure to Daytime and Nighttime Heat Waves in South Asia, *Earth's Future*, *10*(5), e2021EF002511. https://doi.org/10.1029/2021EF002511

Weber, T., A. Haensler, D. Rechid, S. Pfeifer, B. Eggert, and D. Jacob (2018), Analyzing Regional Climate Change in Africa in a 1.5, 2, and 3°C Global Warming World, *Earth's Future*, *6*(4), 643-655. https://doi.org/10.1002/2017EF000714

Weber, T., P. Bowyer, D. Rechid, S. Pfeifer, F. Raffaele, A. R. Remedio, C. Teichmann, and D. Jacob (2020), Analysis of Compound Climate Extremes and Exposed Population in Africa Under Two Different Emission Scenarios, *Earth's Future*, *8*(9), e2019EF001473. https://doi.org/10.1029/2019EF001473

Wegren, S. K. (2013), Food Security and Russia's 2010 Drought, *Eurasian Geography and Economics*, *52*(1), 140-156. https://doi.org/10.2747/1539-7216.52.1.140

Wehner, M., Stone, D., Krishnan, H., AchutaRao, K., & Castillo, F. (2016). The Deadly Combination of Heat and Humidity in India and Pakistan in Summer 2015. *Bulletin of the American Meteorological Society, 97*(12), S81-S86. https://doi.org/10.1175/BAMS-D-16-0145.1

Yin, J., P. Gentine, L. Slater, L. Gu, Y. Pokhrel, N. Hanasaki, S. Guo, L. Xiong, and W. Schlenker (2023), Future socio-ecosystem productivity threatened by compound drought–heatwave events, *Nature Sustainability*, *6*(3), 259-272. https://doi.org/10.1038/s41893-022-01024-1

Yu, R., and P. Zhai (2020), Changes in compound drought and hot extreme events in summer over populated eastern China, *Weather and Climate Extremes*, *30*. https://doi.org/10.1016/j.wace.2020.100295

Yuval, J., & O'Gorman, P. A. (2020). Stable machine-learning parameterization of subgrid processes for climate modeling at a range of resolutions. *Nat Commun, 11*(1), 3295. https://doi.org/10.1038/s41467-020-17142-3

Zhang, G., H. Wang, T. Y. Gan, S. Zhang, L. Shi, J. Zhao, X. Su, and S. Song (2022), Climate Change Determines Future Population Exposure to Summertime Compound Dry and Hot Events, *Earth's Future*, *10*(11). https://doi.org/10.1029/2022EF003015

Zhang, Q., D. She, L. Zhang, G. Wang, J. Chen, and Z. Hao (2022), High Sensitivity of Compound Drought and Heatwave Events to Global Warming in the Future, *Earth's Future*, *10*(11). https://doi.org/10.1029/2022EF002833

Zscheischler, J., et al. (2018), Future climate risk from compound events, *Nature Climate Change*, *8*(6), 469-477. https://doi.org/10.1038/s41558-018-0156-3